

Experimental and theoretical Stark broadening studies of the hydrogen Paschen β line

T. Wujec,* W. Olchawa, J. Halenka, and J. Musielok

Institute of Physics, Opole University, Oleska 48, 45-052 Opole, Poland

(Received 15 January 2002; revised manuscript received 1 October 2002; published 10 December 2002)

Experimental and theoretical Stark broadening studies of the Paschen β line of hydrogen ($\lambda = 1.28 \mu\text{m}$) are reported. Line shape measurements were performed at electron densities of the plasma between $3.5 \times 10^{15} \text{ cm}^{-3}$ and $7.5 \times 10^{15} \text{ cm}^{-3}$, applying as the light source a wall-stabilized arc operated at atmospheric pressure in a helium-hydrogen gas mixture. The radiation of the plasma, emitted from nearly homogeneous plasma layers in the end-on direction, was registered with the use of a grating spectrometer equipped with a charge coupled device detector. The measured light outputs were calibrated against signals obtained from a tungsten strip radiation standard. The experimentally determined line profiles are compared with results of new Stark broadening calculations based on simulation techniques. The measured broadening, shift, and asymmetry parameters are also compared with results of previous Stark broadening calculations and other experimental data obtained at electron densities higher as well as lower than ours.

DOI: 10.1103/PhysRevE.66.066403

PACS number(s): 52.70.Kz, 32.70.Jz

I. INTRODUCTION

As a consequence of the linear Stark effect, spectral lines of hydrogen and hydrogenlike ions emitted from plasmas exhibit significant broadening compared to lines of other plasma constituents. The shapes of these lines depend not only on the specific transition between two energy levels but also on the density of charged particles surrounding the emitting hydrogen atoms or hydrogenic ions. Therefore Stark broadening of these lines is often applied for plasma diagnostic purposes. Particularly, the full widths at half maximum (FWHM) of hydrogen lines of the Balmer series and of the Paschen α transition in He II are frequently used as a measure of electron (ion) density in plasmas. Hydrogen spectral lines of the Balmer series have been the subject of numerous experimental as well as theoretical investigations, because of their convenient location in the visible part of the waveband. The number of experimental studies devoted to transitions belonging to other spectral series is rather scarce. In the case of Lyman lines the main experimental difficulties are the radiation detection in the vacuum and the self-absorption processes in the plasma, while in the case of the Paschen lines their rather weak intensities, the light absorption by traces of water vapors in the atmosphere and the problems arising from detection of low-energy photons.

To our knowledge, only in a few papers published to date are experimental line broadening data for hydrogen transitions of the Paschen series reported [1–4].

Hepner's single measurement for the Paschen β line (P_β) [1] was derived from studies of a capillary discharge in hydrogen at an electron density somewhat above 10^{16} cm^{-3} . The P_β line profile was determined by scanning the wavelength on a shot-by-shot basis, relying on the reproducibility of the discharge.

The results reported by Castell *et al.* [2] are also based on the above-mentioned measuring technique. The discharge was conducted in helium with traces of hydrogen at a pres-

sure of 0.4 mtorr. Profile measurements of the P_β line in the electron density interval from 3.6×10^{14} to $2 \times 10^{15} \text{ cm}^{-3}$ are reported. The analysis of this paper leads to the following remarks:

(i) As reported by the authors, the measured spectra were significantly disturbed by two strong He I transitions (in the blue wing of P_β) and by other impurity lines.

(ii) In the results presented in the paper in Figs. 5–7, line shapes are obtained after some corrections, which are required in order to remove the above-mentioned disturbance (the captions of Figs. 5 and 7 should be obviously exchanged).

(iii) In spite of these corrections, the experimental data (represented by about 40 measuring points on each line profile) still exhibit a significant scatter, which may only partly be attributed to the disturbance arising from the Ar I line at 12802.7 \AA —the spectral lines that appear in the red wing of the P_β can be attributed neither to argon atoms nor to ions.

Thus one may conclude that the P_β broadening data of Castell *et al.* are very uncertain.

The most comprehensive and reliable measurements, concerning the P_β line profiles, have been recently reported by Döhrn [3] and Döhrn *et al.* [4]. The authors applied a wall-stabilized arc running in neon or argon always with some amount of hydrogen. The arc was operated at different pressures ranging from 1 to 6 atm. Line shapes were determined at several plasma conditions ranging from $N_e = 5 \times 10^{15}$ to $N_e = 10^{17} \text{ cm}^{-3}$. At these electron densities, the FWHM of the P_β line range from about 45 to nearly 500 \AA . At the higher N_e values, the argon and neon background lines exhibited remarkable Stark broadening. One of the critical points of these measurements was the subtraction of the neon or argon background. In order to obtain reliable P_β line profiles, it is necessary to perform measurements in a waveband significantly wider than the FWHM of the P_β . Particularly, the unknown spectral feature around $1.26 \mu\text{m}$, observed in the neon discharge, was a considerable disturbing factor. Moreover, at plasma conditions with higher N_e , a significant overlap of the blue wing of P_β and the red wing of P_γ line, with its center at 10938 \AA , has to be expected. Thus, one

*Electronic address: wujec@uni.opole.pl

may conclude that in evaluating P_β line profiles, the authors have encountered severe difficulties not only arising from the subtraction of the *foreign* background (unidentified feature, neon and argon bound-bound emission) but also from the determination of the *true* continuum.

Theoretical studies of Stark broadening of hydrogen lines from the infrared part of the spectrum are scarcely available in the literature, either. Calculations of hydrogen P_β line shapes have been reported in four recent publications.

The so-called global theory of Motapon *et al.* [5] is based upon a quasimolecular treatment of the problem of line broadening developed earlier in Refs. [6,7]. Numerical calculations of line profiles are executed within the adiabatic approximation. The evaluated half-widths of the lines are generally in a satisfactory agreement with results of quasi-static semiclassical calculations, e.g., Refs. [8,9], while the line shapes differ remarkably. Unfortunately, for determination of line profiles, suitable for comparison with experimental data, several significant simplifications of the applied approach are unavoidable.

In the paper of Stehle [10] and of Stehle and Hutcheon [11], the model microfield method (MMM) has been applied for both the electronic as well as the ionic contribution, with protons considered as the heavy perturbing particles. The dynamics of microfield fluctuations are treated by a statistical process model, where the microfield (electronic or ionic) is assumed to be constant during a given time interval. The microfield then jumps instantaneously to another constant value for the next time interval. In practice, the calculations of P_β [11] have been carried out neglecting the broadening of the lower ($n=3$) level of the transition and applying the so-called isotropic approximation. The half-widths—including Doppler broadening—have been determined for electron densities ranging from 10^{10} to 10^{19} cm^{-3} and for a set of temperature values, e.g., suitable for application to typical stellar envelopes. The MM-method yields FWHM values, which are in between the results of quasistatic approximations for ions [8,9] and those of the full computer simulation method (FCSM) [12–15]. In the case of β -like transitions, the discrepancies are rather small. In the case of α -like transitions in hydrogen, significantly larger discrepancies are encountered between the results of MMM on one hand and the FCSM and experiments on the other, e.g., Refs. [12,13]. A similar conclusion can be drawn from studies of α -like transitions for ionic emitters [16,17].

In the paper of Döhrn *et al.* [4], the quantum statistical approach using the Green's functions technique, developed earlier by Günter and co-workers [18–20], has been applied for the treatment of perturbing electrons, and the MMM to include the contribution from dynamical plasma ions. Calculations of the ion dynamics are based—similarly as in Refs. [10,11]—upon a modeling of the statistics of time fluctuations of the ionic microfield.

In the electron density interval $3 \times 10^{14} - 10^{17}$ cm^{-3} , the calculations of Döhrn *et al.* [4] yield a similar linear dependence of the logarithm of the FWHM on the logarithm of N_e as the approach of Stehle and Hutcheon [11]. At an electron density of 4×10^{14} cm^{-3} , both calculations yield the same FWHM. The slope of this dependence is somewhat larger in

the case of Ref. [11]. The discrepancy between the FWHM at $N_e = 10^{17}$ cm^{-3} does not exceed 10%.

Such a relatively good agreement between these calculations is not surprising since the FWHM of β -like transitions is rather insensitive to different theoretical approaches. In this paper we present results of new P_β line shape calculations, based on computer simulation techniques described and analyzed in detail in Refs. [13,21]. Calculations of Ly_α line profiles (the most sensitive transition to ion-dynamic effects) reveal that this technique yields results that agree very well with experimental data [12–15, 21–25]. The computer simulation technique includes the ion-dynamic effects in a complete and natural way, in contrast to the MMM, where this effect is considered only approximately. The simulated positions and movements of perturbers are simply determining the plasma microfields and their time variations.

Our theoretical results are compared with measured line profiles at electron densities from 3.5×10^{15} to 7.5×10^{15} cm^{-3} . This N_e interval—at temperatures typical of arc discharges ($T \approx 1 \times 10^4$ K)—seems to be most appropriate for verifications of Stark broadening of the hydrogen P_β transition. At these plasma conditions, the line exhibits large enough Stark broadening, exceeding significantly the contribution from the Doppler effect. On the other hand, the Stark broadening is not too large, therefore reliable line profile measurements are possible, including intermediate line wings (the problems arising from difficulties in the determination of the continuum radiation are minimized).

II. THEORETICAL APPROACH

Our P_β calculations are performed assuming classical straight paths for the perturbers. The FCSM has been applied, i.e., the time variation of the total microfield at the radiator's position produced by ions as well as by electrons is simulated. Our calculations are based on the approach and formalism described in detail by Halenka and Olchawa [13,21]. The starting point of this consideration is the relation between the spectral line profile and the average of the dipole autocorrelation function $C(t)$, which can be written in the following way:

$$I(\omega) = \lim_{t_f \rightarrow \infty} \pi^{-1} \text{Re} \int_0^{t_f} C(t) e^{i\Delta\omega t} dt, \quad (1)$$

$$C(t) = \text{Tr}\{\mathbf{d}_{if} \cdot U_{ff'}^\dagger(t) \mathbf{d}_{f'i'} U_{i'i}(t)\}_{av} / \text{Tr}\{\mathbf{d}_{if} \cdot \mathbf{d}_{fi}\}, \quad (2)$$

where \mathbf{d} is the dipole operator for the hydrogen atom, while ii' and ff' indicate the sublevels of the initial (E_i) and final (E_f) states of the unperturbed atom, respectively. The frequency separation from the line center is given by $\Delta\omega = \omega - (E_i - E_f)/\hbar$, whereas $U(t)$ is the operator of the time development of the hydrogen atom in the presence of the electric field produced by electrons and ions. The averaging $\{\dots\}_{av}$ is taken over all initial simulated field strengths and possible time histories. The time-evolution operators $U_{i'i}(t)$ and $U_{f'f}(t)$ (corresponding to the initial and final states, respectively) satisfy the following Schrödinger equation:

$$i\hbar \dot{U}(t) = [H_0 + V(t)]U(t), \quad (3)$$

where H_0 is the Hamiltonian of the isolated radiator and $V(t)$ is the radiator-plasma interaction potential.

The Hamiltonian, with the multipole expansion of the potential restricted to quadrupole terms, may be written (e.g., Ref. [26]) as follows:

$$H(t) \approx H_0 - \mathbf{d} \cdot \mathbf{F}(t) - (1/6) \sum_{j,k} Q(t)_{jk} F_{jk}(t), \quad (4)$$

where the second term in Eq. (4) describes the plasma-emitter dipole interaction and the third represents the quadrupole interaction of the radiator with the inhomogeneous electric microfield of the plasma. The electric field $\mathbf{F}(t)$ and the inhomogeneous microfield tensor $F_{jk}(t)$ represent the respective total fields originating from ions and electrons.

The perturbers are moving along straight trajectories with velocities calculated according to the Maxwell distribution. We applied the so-called μ^* -ion model introduced by Kesting [15]. Kesting demonstrated there, that exact calculations in the frame of the so-called collision time statistics [14] are well reproduced by the μ^* model, which is convenient in applications. This model allows—using a coordinate system bound to a statistical emitter—to treat the plasma as an isotropic medium. In this model the coupling between Stark and Doppler broadening is taken into account, in contrast to the usually used μ -ion model, where this coupling is ignored. Our calculations differ from the Kesting's model in two points: (i) we restrict the radius of the simulation sphere to $3D$ (D being the electronic Debye radius), and (ii) for electrons we use the cutoff Coulomb field for $\rho \geq D$ (ρ being the collision parameter), instead of the screened Debye potential applied in Refs. [14,15]. Detailed studies of the point (i) performed in Refs. [13,21] reveal that the influence of weak collisions on line profiles, i.e., collisions with impact parameters more distant than $3D$, is negligibly small. Our technique of substituting those perturbers that are moving away from the simulation sphere differ somewhat from the technique applied in Refs. [12,23], and are described in Refs. [13,21]. The cutoff problem mentioned in (ii) has been studied, e.g., by Smith [27]. From this study one may conclude that the cutoff Coulomb potential, used for description of the electric field produced by electrons, correctly reproduces the electron-electron correlations. The choice of the potential shape does not influence considerably the final line profile—the application of either the cutoff Coulomb potential or the shielded Debye potential leads to almost the same results. Such comparison is presented in Fig. 4(a) of Ref. [13]. Since in our simulations we consider the perturbers as classical particles, we also encounter the problem of the treatment of strong collisions. We assume that the emitter is a rigid sphere with a radius equal to the radius of the upper orbit of the respective level: $R_{min} = 3/2 a_0 n_i^2$, where a_0 is the Bohr radius. This question will be discussed in further parts of this paper. Our simulations differ from those of Refs. [14,15] also in some technical details. Following the recommendation contained in Ref. [28], we applied Fehleberg's adaptive-

stepsize method for integration of differential equations, instead of the predictor-corrector method of Adams, which were used in Refs. [14,15].

Calculations

In the frame of the above-mentioned model we attempted to determine P_β line shapes including their shifts and asymmetries. Therefore, in the Hamiltonian [see Eq. (4)], we have taken into account the nonhomogeneity of the local microfield including quadrupole terms. The calculations of line profiles have been executed with accuracy up to the dynamic quadratic Stark effect. Unfortunately, even after averaging of 10 000 initial perturber configurations, the resulting statistical noise of the imaginary part of the autocorrelation function, $\text{Im } C(t)$, did not allow to determine reliable asymmetries and shifts of the profile. Furthermore, the resulting imaginary part of the autocorrelation function, $\text{Im } C(t)$ [calculated by applying the Hamiltonian, Eq. (4)] depends on the chosen R_{min} value, i.e., on the assumed radius of the emitter. It is the weakest point of our calculations. Also in analytical approaches within the so-called classical trajectory approximation for perturbers, the same difficulty occurs—one has to assume (somewhat arbitrarily) the collision parameter ρ_{min} . Iglesias *et al.* [29] have shown that the electronic shift calculated by Griem [30] within the semiclassical binary impact approximation (originating from electron-emitter interactions) strongly depends on the assumed collision parameter ρ_{min} . This strong dependence indicates that the contribution to the line shift from strong collisions is significant and has to be treated quantum mechanically. In our opinion, the electronic shift of hydrogen spectral lines is well described within the statistical approach using the Green's function technique, *see* Refs. [20,25]. Calculations performed by Günter and Könies [31] reveal that the asymmetry of line profiles caused by electron-emitter interactions is negligible compared to the asymmetry produced by ion-emitter interactions. Thus it is reasonable to assume that electron-emitter interactions produce only a pure redshift $\delta\omega_e$ of the line. With this assumption, the line profile may be described in the following way:

$$I(\Delta\omega) = I^{(d)}(\Delta\omega') + \Delta I(\Delta\omega'), \quad (5)$$

where $\Delta\omega' = \omega - \omega_0 - \delta\omega_e$ is the separation frequency; $I^{(d)}(\Delta\omega')$ represents the symmetrical line profile obtained within the dipole approximation, calculated with accuracy up to the linear Stark effect, while $\Delta I(\Delta\omega')$ include the contributions to the profile originating from higher-order terms, describing the interaction of the emitter with the ionic microfield.

The symmetrical parts $I^{(d)}(\Delta\omega')$ have been determined according to our FCSM. We want to emphasize that within the dipole approximation the autocorrelation function $C^{(d)}(t)$ of the profile $I^{(d)}$ is real. The imaginary part of the function, $\text{Im } C^{(d)}(t)$, is equal to zero, i.e., within this approximation the profile is not shifted. Each line profile was determined on the basis of 3000 perturber configurations taken for averaging. The analysis of the accuracy of our calculations has been carried out according to the procedure outlined in detail in

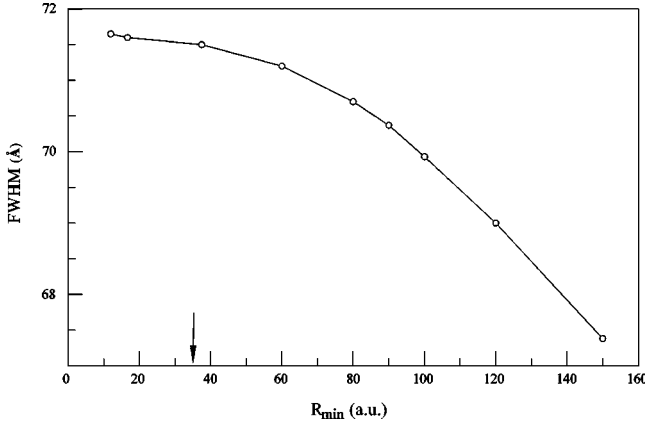


FIG. 1. The FWHM of the P_β line versus the radius of the sphere representing (in our FCSM calculations) the size of the emitter for the plasma conditions $N_e = 6.3 \times 10^{15} \text{ cm}^{-3}$ and $T = 10\,000 \text{ K}$. The arrow shows the average radius of the orbit for $n=5$, i.e., the initial state for the P_β transition.

Ref. [13]. The statistical uncertainty of the determined FWHM is estimated to be less than 3%. The uncertainty of the intensity course in the line core, however, is larger but does not exceed 10%.

Since we applied the classical trajectory approximation for perturbers, it was necessary to estimate the contribution to the line broadening originating from strong collisions. Thus, for a given set of experimental conditions, we calculated the profiles $I^{(d)}(\Delta\omega')$ for various values of the sphere radius R_{min} , which represent different sizes of the emitter. These calculations reveal that the real part of the autocorrelation function, $\text{Re } C(t)$ (in the dipole approximation), only insignificantly depends on the assumed R_{min} value, while the imaginary part $\text{Im } C(t)$ is equal to zero. In Fig. 1 the determined FWHM versus the assumed R_{min} are presented. As can be seen, even for R_{min} approaching zero, our FCSM yields FWHMs, which are close to those obtained for $R_{min} = 37.5a_0$, i.e., for the radius of the fifth orbit of the hydrogen atom. Thus, one may conclude that in the case of the P_β line, the contribution to the line broadening originating from strong collisions is negligibly small. The above described procedure of estimation of the contribution of strong collisions to the FWHM yields some information about the upper limit of this contribution. Generally, it is not easy to include interactions with small collision parameters, because for such collisions some effects become important (e.g., the penetration effect [32]), which introduce mathematical difficulties. Within the electron cloud of the emitter, a short-range potential appears, which always reduces the long-range dipole potential. Thus the neglect of this short-range potential always leads to an overestimation of the perturbation. In addition, we have proved that the procedure of integration of the Schrödinger equation, Eq. (3), yields results that obey the probability conservation law, i.e., for each integration step, the matrices of the time evolution are unitary. Even very strong collisions yield absolute values of the matrix elements not exceeding the value of 1.

The correction to the profile $\Delta I(\Delta\omega')$ has been determined by applying the quasistatic approximation for ions and

the impact approximation for electrons. The Stark broadened line profile may be, in this approximation, expressed in the following form [8]:

$$I_{qs}(\Delta\omega') = \frac{1}{\pi} \text{Tr} \int_0^\infty d\beta W_\rho(\beta) \mathbf{d}_{if} \cdot \mathbf{d}_{f'i'} \times \langle if | [i\Delta\omega' - i(H_{n_i} - H_{n_f})/\hbar - \Phi_{n_i, n_f}]^{-1} | i'f' \rangle, \quad (6)$$

where $W_\rho(\beta)$ is the probability density of the ionic component of the local microfield [33] in the reduced scale $\beta = F/F_0$, where $F_0 = e_0/R_0^2$ is the Holtsmark normal field, while R_0 is the mean distance between them, resulting from the relationship $(4\pi/3)R_0^3N_e = 1$. The symbol Φ represents the electronic impact operator. In our calculations, the interference term Φ introduced by Kepple and Griem [8] has been properly corrected. In the quasistatic approximation for ions, the Hamiltonian given by Eq. (4) may be written (e.g., Ref. [26]) as

$$H = H_0 + V_{qs} \approx H_0 + e_0F_0\beta z - \frac{5}{(32\pi)^{1/2}} \frac{e_0F_0}{2R_0} \times B_\rho(\beta)(3z^2 - r^2), \quad (7)$$

where $B_\rho(\beta)$ is the generalized Chandrasekhar–von Neumann function, calculated in Ref. [26]. The correction of the profile $\Delta I(\Delta\omega')$ has been determined as the difference between two quasistatic profiles:

$$\Delta I(\Delta\omega') \approx \Delta I_{qs}(\Delta\omega') = I_{qs}(\Delta\omega') - I_{qs}^{(d)}(\Delta\omega'). \quad (8)$$

For the determination of the profile $I_{qs}(\Delta\omega')$, the matrix elements of all operators in Eq. (6) have been calculated with accuracy up to the quadratic Stark effect. The profile $I_{qs}^{(d)}(\Delta\omega')$ has been calculated applying the dipole approximation for emitter-ion interactions ($V_{qs} = e_0F_0\beta z$) with accuracy up to the linear Stark effect, i.e., with the same accuracy as the profile $I^{(d)}(\Delta\omega')$ calculated in the FCSM approximation.

It is well known that the quasistatic approximation may be successfully used in the profile range, where the following relation is valid, e.g., Ref. [34]:

$$|\Delta\omega'| \gg v_i/R_i \equiv \Omega_i, \quad (9)$$

where $v_i = (8kT/\pi m_i)^{1/2}$ is the mean thermal velocity of ions while R_i is the mean distance between them, resulting from the relationship $(4\pi/3)R_i^3N_i = 1$. For all P_β line shapes measured in this paper, the distance between the peak and the center of the line (in $\Delta\omega$ units) exceeded the value Ω_i defined in Eq. (9) by a factor of 2. Thus one may infer that the quasistatic approximation is justified for the outward parts of the profile, including the line peaks with exception of only its very central range close to the line dip. Fortunately, around the line dip, where the quasistatic approximation is not valid, the correction to the profile $\Delta I(\Delta\omega')$ is relatively small (compared to other parts of the profile), because the central

part is formed by weak electric microfields (compared to the mean field $F_i = e_0/R_i^2$). Therefore the application of the quasistatic approximation practically does not influence the accuracy of the determination of the final profile $I(\Delta\omega)$. On the other hand, the impact approximation may be applied in the central range of the profile up to frequency separations obeying the relation (e.g., Ref. [34])

$$|\Delta\omega'| \ll v_e/R_0 \equiv \Omega_e, \quad (10)$$

where v_e is the mean thermal velocity of electrons. For all measured P_β line shapes, the inequality [Eq. (10)] is well fulfilled in the frequency range comprising at least four half-widths at half maximum (HWHM). For all plasma conditions of our experiments, the frequency Ω_e exceeded the HWHM at least by a factor of 5. Thus one may conclude that the introduced correction of the profile in Eq. (5), $\Delta I(\Delta\omega')$, applying the quasistatic approximation for ions and impact approximation for electrons, is justified.

III. EXPERIMENT AND PLASMA DIAGNOSTICS

A. Experimental setup and radiation detection

A wall-stabilized arc running at atmospheric pressure was applied for our studies. The details of the arc construction can be found elsewhere [35], therefore only a few essential remarks concerning some peculiarities of this experiment will be given below. The arc channel of a diameter of $\phi=4$ mm and a length of 70 mm is formed by a stack of nine water-cooled copper plates. The central part of the arc column (about 80% of the total plasma length) was operated in a mixture of helium and hydrogen, while the regions close to both electrodes were supplied additionally with very small amounts of argon in order to improve the stability of the discharge. The arc was operated at five different arc currents: 20, 25, 30, 35, and 40 A. The advantages of running the arc in helium with small amounts of light elements, for studying the admixture spectra, have been discussed in detail, e.g., in Refs. [36,37]. From the point of view of this particular study, the plasma source has the following main advantages:

(i) The arc operated in a mixture of helium and hydrogen yields effective population of the respective upper level of hydrogen ($n=5$) at moderate electron densities and thus produces large spectral intensities within the P_β line.

(ii) Only a few weak bound-bound transitions of neutral helium and argon appear in the range of the P_β emission, the strongest line of them—at conditions of our experiments—was the Ar I line at $\lambda = 12\,802$ Å, i.e., 15 Å away from the center of the P_β line.

(iii) At our moderate electron densities, the He I and Ar I lines are very narrow (almost negligible Stark broadening), and thus the measured hydrogen spectrum can be easily set free from this disturbance.

(iv) The continuum background radiation is very weak, facilitating the determination of the P_β line shape including the intermediate line wings.

The scheme of the spectral instrumentation is shown in Fig. 2. The arc emission was observed in the end-on direction. The large focal length ($f=730$ mm) of the concave

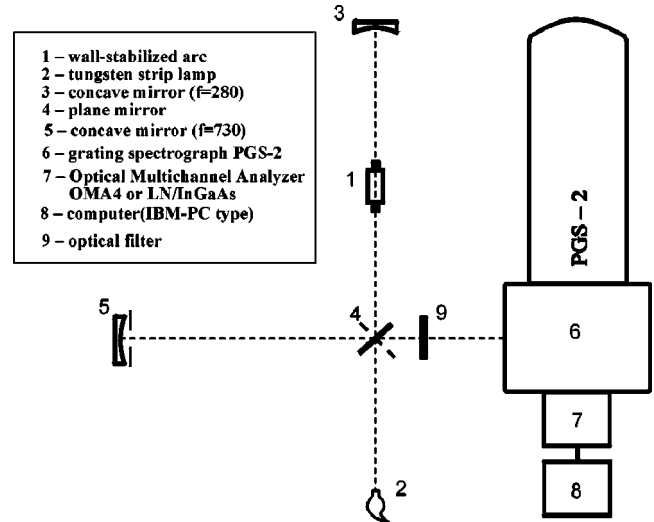


FIG. 2. The scheme of the experimental setup.

mirror (5) and the small diameter of the diaphragm in front of it ($\phi=12$ mm) enabled us to select the radiation originating from nearly homogeneous plasma layers (fixed N_e and T) parallel to the arc axis. The spatial resolution of our instrumentation was 0.25 mm. The homogeneity of individual plasma layers was controlled by determining the ratio between the FWHM and the peak separation of both measured β -like hydrogen lines. Using the concave mirror (3), the radiation emitted in the direction opposite to the spectrometer could be reflected back through the plasma column. In this way, self-absorption checks were performed, showing that at conditions of our experiments the light absorption in the arc was negligibly small for all measured line profiles. Nevertheless, the very small self-absorption in the line centers of both studied hydrogen lines (spectral intensities reached there merely 2% of the Planck function value) was taken into account in the determination of the line profiles. By changing the angular position of the plane mirror (4), the emission of the tungsten strip radiation standard lamp could be detected. In this manner, our arc emission was calibrated. The radiation emitted by the arc and the standard lamp was analyzed applying a grating spectrograph PGS-2 equipped with exchangeable gratings having 651 grooves/mm. The spectra were recorded with two exchangeable charge coupled device detectors mounted in the exit focal plane of the spectrograph. In the visible and near-infrared part of the spectrum, a grating blazed at 7400 Å and a two-dimensional optical multichannel analyzer (OMA4) with 1024×256 individual pixels ($19 \times 19 \mu\text{m}^2$) were applied. For the P_β measurements, a grating blazed at 10 800 Å and a liquid nitrogen cooled InGaAs photodiode linear array detector (LN/InGaAs), consisting of 512 individual rectangular pixels ($250 \mu\text{m}$ in the direction perpendicular and $38 \mu\text{m}$ parallel to the dispersion) were used. The distances between two subsequent pixels along the dispersion are $25 \mu\text{m}$ and $50 \mu\text{m}$ for the OMA4 and LN/InGaAs detector, respectively. The IR detector is sensitive in the spectral range from 8000 Å up to 17 000 Å and exhibits a *flat* characteristic in the waveband 9500–16500 Å. With this instrumentation, spectral intervals of about 180 Å could be simultaneously registered in the

visible and infrared parts of the spectrum. The FWHM of the instrumental profiles were 0.7 \AA for the P_β measurements and 0.56 \AA for detection in the visible and near-infrared wavelength range. These instrumental widths were determined experimentally by recording the radiation emitted from a low-pressure Plücker-type discharge in hydrogen. The Plücker tube also served as a standard source for wavelength calibration of our measured spectra. The registration of the arc radiation originating from different but nearly homogeneous layers of the plasma column (parallel to the arc axis) was accomplished: (i) In the case of the detection in visible and near-IR part of the spectrum by dividing the OMA matrix into adequate tracks, assuring the required spatial resolution; and (ii) In the case of the P_β measurements by placing the detector at the respective position in the exit focal plane of the spectrometer (the position of the detector corresponds to a certain plasma layer in the arc).

B. Plasma diagnostics

For studies of Stark broadening of the P_β line, the most significant plasma parameter is the electron density. In order to determine this parameter we have recorded the shape of the Balmer β (H_β) line and measured the respective FWHM. Subsequently, the contributions originating from Doppler and instrumental broadening have been subtracted and the pure Stark widths are obtained. For determination of electron densities of the plasma, the theoretical broadening data of Gigoso and Cardenoso [12(c)] have been used.

According to equilibrium criteria [38], at electron densities of our experiments, the assumption of partial local thermodynamic equilibrium is justified for all atomic levels with principal quantum numbers $n \geq 3$. Thus, in order to determine the plasma temperature by the Boltzmann plot method, we have additionally introduced into the discharge volume small amounts of nitrogen and detected the spectrum around 9050 \AA . In this wavelength interval the spectral lines of two neutral nitrogen (NI) multiplets appear: $3p^2S^0 - 3d^2P$ and $3s'^2D - 3p'^2F^0$. The excitation energy gap between the upper terms of these multiplets is 0.85 eV , which is sufficient for evaluation of the plasma temperature. The corresponding transition probabilities of the fine structure components were taken from Ref. [39]. The temperatures obtained in this way for different plasma layers and different arc currents are in the range between 8000 and $11\,000 \text{ K}$. The electron densities of the corresponding plasma layers are between 3.5×10^{15} and

$7.5 \times 10^{15} \text{ cm}^{-3}$. At the plasma composition and temperatures of our experiments, the bulk of free electrons originate from ionized hydrogen atoms. Thus the P_β line shapes are predominantly formed by interactions of hydrogen atoms with singly ionized particles (protons, $\mu = 0.5$) and electrons. The measurements for diagnostic purposes (H_β and NI multiplets) were accomplished by applying the OMA4 detector and the grating blazed at 7400 \AA .

IV. RESULTS AND DISCUSSION

As mentioned above, our P_β line shape studies have been performed at different plasma conditions. These different

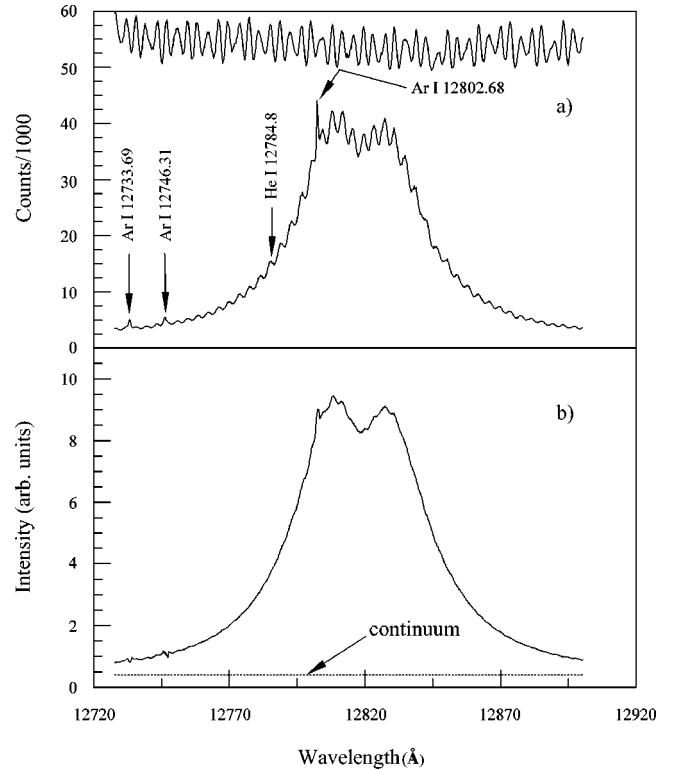


FIG. 3. Illustration of the smoothing procedure applied to our measured spectra for determination of line profiles and the continuum background radiation: (a) directly measured signals from the arc discharge (P_β line) and from the standard source (upper signal); (b) the P_β line shape after applying the smoothing procedure based on the Fourier transform technique and after the radiance calibration; the dashed line represents the continuum level determined according to the procedure outlined in Eq. (11).

conditions were accomplished by (i) running the arc at different currents (20, 25, 30, 35, and 40 A) and (ii) selecting appropriate plasma layers at various distances from the arc axis. For each plasma condition, at least four independent spectra were taken for three different wavelength intervals, comprising the line shapes of P_β , H_β , and additionally the NI spectrum around 9050 \AA , used for temperature determination. The main advantage of our P_β line shape measurements is the registration of the whole profile during a single exposition lasting less than 1 s. The very good stability of the arc discharge enabled us to change the angular position of the grating for check measurements of the shape of the far P_β line wings, and subsequently replace the grating and the multichannel detector in order to measure the spectra in the visible (H_β) and near IR part of the spectrum (NI), suitable for N_e and T determination.

As an example, in Fig. 3(a) the measured line shape of the P_β line is shown. Above the P_β shape, the corresponding light output from the standard source is presented. From both measured light outputs, only the respective dark currents have been subtracted. As can be seen, both relative strong signals are superimposed by a remarkable and regular interference pattern. The amplitude of this characteristic feature is proportional to the light intensity, and is—in this wavelength range—of the order of 5% of the light output. (In the visible

part, this disturbance is significantly weaker.) In order to release the measured signals from this disturbing interference pattern, the directly recorded spectra were filtered applying the Fourier transform technique. The transformation revealed two characteristic *frequencies* responsible for this characteristic interference pattern. These frequencies are characteristic for our spectroscopic instrumentation and depend on the wavelength but not on the light intensity. After smoothing the respective parts of the Fourier transform spectrum, the released P_β line shapes were evaluated by retransforming the data into real spectra. The result of this smoothing procedure is shown in Fig. 3(b). As can be seen, the smoothing procedure removes significantly the regular interference pattern, yielding satisfactory P_β line shapes, but also considerably alter the intensity of narrow spectral lines, having widths comparable to the width of a single interference peak. Therefore this smoothing procedure may only be applied for evaluation of spectral features much broader than the characteristic widths of the interference peaks. After applying the smoothing procedure, the measured arc signals were calibrated using the corresponding light outputs of the standard source. Subsequently, the course of the underlying continuum radiation was determined [the dashed line in Fig. 3(b)]. On the basis of theoretical premises, we assumed that the wings of the P_β line exhibit power-law-like shapes. The continuum was approximated by a function depending linearly on wavelength. With these assumptions, the distribution of the spectral intensity—in wavelength intervals corresponding to the P_β line wings—can be written in the following form:

$$J(\Delta\lambda) = a_v |\Delta\lambda|^{b_v} + a_c \Delta\lambda + b_c \quad \text{for the violet wing,}$$

$$J(\Delta\lambda) = a_r (\Delta\lambda)^{b_r} + a_c \Delta\lambda + b_c \quad \text{for the red wing.} \quad (11)$$

where $\Delta\lambda = \lambda - \lambda_0$, with λ_0 being the wavelength of the dip of the P_β . The parameters for the wings (a_v, b_v, a_r, b_r) as well as for the continuum (a_c, b_c) were determined by a least-squares-fitting procedure, on the basis of measured spectral intensities corresponding only to the outward parts of the P_β line profile, for which the outputs did not exceed 1/8 of the maximum spectral line intensity. The correctness and reliability of our fitting procedure was confirmed by a few tests, in which we extended our measurements to shorter as well as longer wavelengths than shown in Fig. 3. The same procedure was applied for the evaluation of H_β line profiles. For all the analyzed H_β and P_β line shapes, the fitting procedure yielded b_v and b_r exponents in the range from -2.3 to -2.2 . As expected, these values are in between those characteristic of Holtsmark (-2.5) and Lorentz (-2.0) profiles.

The relationship between the line profile $I(\Delta\omega)$ and the spectral line intensity distribution $J(\Delta\omega)$ can be written [26] as

$$J(\Delta\omega) = J_0(\omega_0) (1 + \Delta\omega/\Delta\omega_0)^4 \exp(-\hbar\Delta\omega/kT) I(\Delta\omega). \quad (12)$$

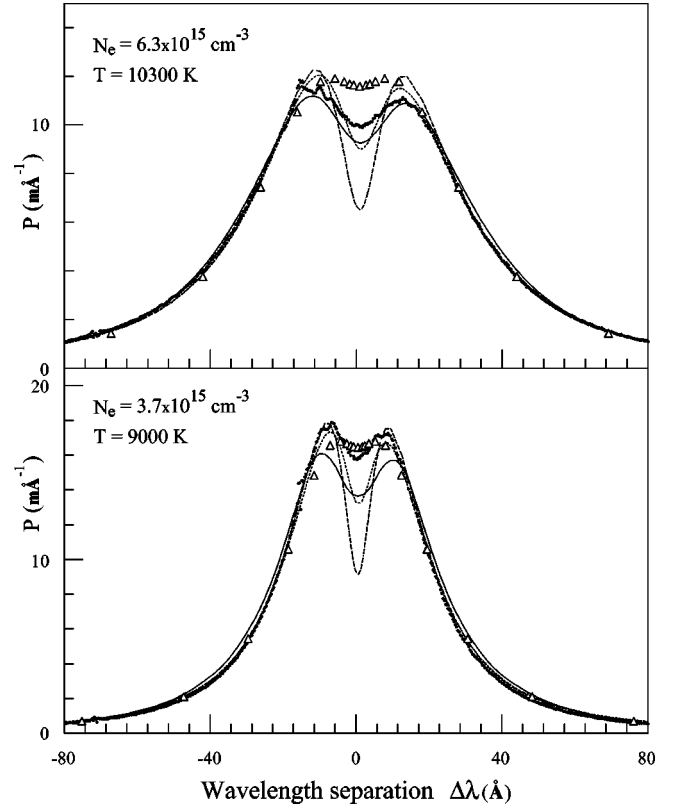


FIG. 4. Comparison of experimentally determined P_β line profiles with our calculations and other theoretical results for two plasma conditions. The line profiles are area normalized. In the normalization of our experimental profiles, we included the contribution from the line wings according to Eq. (11). The theoretical data are marked by the following symbols and lines: Δ stands for Ref. [11]; \cdots stands for Ref. [31]; $---$ stands for our quasistatic calculations; and $---$ for our FCSM results.

The factor in front of $I(\Delta\omega)$ introduces an additional asymmetry, the so-called trivial asymmetry, which we have taken into account in the analysis of our data, particularly in comparisons of measured and calculated line asymmetries and shifts.

In Fig. 4 the experimentally determined P_β line profiles for two selected plasma conditions: $N_e = 3.7 \times 10^{15}$ and $6.3 \times 10^{15} \text{ cm}^{-3}$ are compared with those determined by our simulation technique and by other theoretical approaches. All line shapes shown in the figure are normalized to the area under the respective profiles. In the case of the measured profiles, the contribution from far line wings, which are not shown in the figure, has been included according to the procedure outlined by Eq. (11). The wavelength separation $\Delta\lambda = 0$ corresponds to the unperturbed position of the P_β line. The calculations of Stehle and Hutcheon [11] do not provide line shifts, therefore the dips of their profiles are positioned at the corresponding dip positions of our experimental profiles. In the case of the higher N_e plasma condition ($6.3 \times 10^{15} \text{ cm}^{-3}$), the overall agreement between our calculated and measured P_β line profile can be considered satisfactory. The apparent discrepancies in the line core may be—at least partly—caused by uncertainties in the determi-

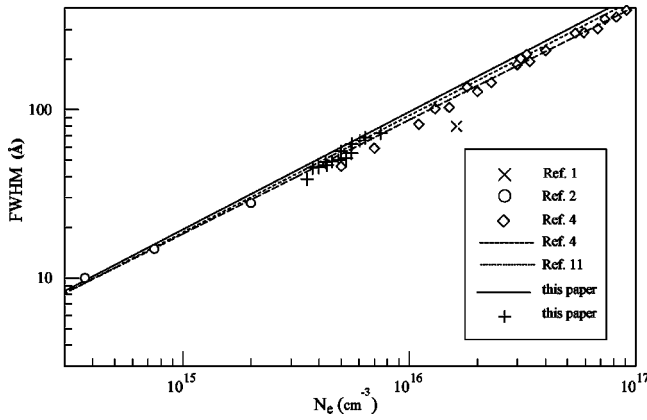


FIG. 5. Comparison of our measured and calculated FWHM of the P_β line with other experimental and theoretical data. The measured data are represented by various symbols while theoretical results are represented by lines.

nation of the continuum level, which influences the normalization procedure. At the *violet* shoulder, the disturbance originating from the Ar I line is visible. The calculated FWHM exceeds the experimental one by about 5%. In the case of the lower N_e condition ($3.7 \times 10^{15} \text{ cm}^{-3}$), it is clearly seen that the experimental shoulder peaks are closer in wavelength than the calculated ones. Also the measured FWHM is remarkably (by about 10%) smaller than that predicted by our simulations. In Fig. 4 our profiles are also compared with results of other theoretical approaches: our quasistatic approximation (Kepple-Griem approximation [8] with corrected interference term), the results of Stehle and Hutcheon [11] and the quantum statistical approach using the Green's function technique of Günter and Könies [31]. As expected, the largest discrepancies are encountered in the line center—the quasistatic approximation predicts the most pronounced line dip, while the approach of Stehle and Hutcheon [11] yields an almost flat profile in the line core. The theory of Günter and Könies [31] yields systematically somewhat more pronounced line core features compared to our calculations. In the case of the higher N_e plasma condition, the overall agreement between the profiles of Ref. [31] and our measured as well as calculated profiles may be regarded as satisfactory. For the lower N_e condition, the discrepancies in the line core become remarkably larger. The significant discrepancy between the results of Refs. [11] and [31] is a little surprising, since in both approaches the MMM has been applied for the treatment of ions.

In Fig. 5 our experimental and calculated FWHM are compared with other available experimental data and with results of recent calculations for a wide range of electron density. Our measured FWHM are systematically slightly smaller than those obtained from our calculations. The discrepancies are evidently larger at lower electron densities. Perhaps the most important reason for this regular behavior is the possible departure of our plasma layers from homogeneity. The lower N_e conditions are realized at lower arc currents and more distant plasma layers from the arc axis, where the radial plasma parameter gradients are stronger. Since our detection system integrates over a fixed *height* of plasma

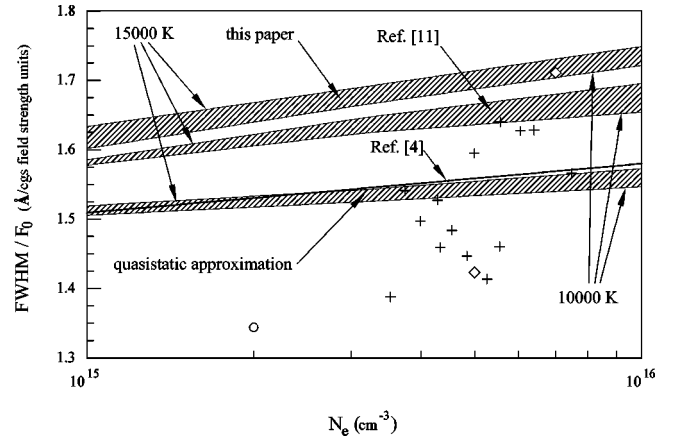


FIG. 6. Comparison of the reduced P_β FWHM calculated and measured (crosses) in this work, with results of other available theoretical and experimental data: \diamond , Döhrn *et al.* [4]; \circ , Castell *et al.* [2]. The upper boundary of each marked area corresponds to results obtained for $T=15\,000$ K, while the lower one corresponds to those for $T=10\,000$ K. The theoretical data of Döhrn *et al.* [4] correspond to temperatures of their experimental conditions.

layers (limited spatial resolution), the departure from homogeneity is expected to be larger for plasma layers with lower N_e . Moreover, our measurements are also influenced somewhat by the radiation originating from arc regions close to the electrodes, where the plasma conditions differ from those of the central part of the arc column. In this way the discrepancy in the line core at the lower N_e condition (Fig. 4), particularly the smaller observed peak separation, may also be explained (see also Fig. 7).

The FWHM of Stark broadened hydrogen spectral lines is often quoted in the so-called reduced scale units $\alpha = \Delta\lambda/F_0$, with F_0 being the normal electric field strength. The advantage of such presentation is that even small differences in the FWHM may be shown in a single graph simultaneously for a relative wide range of electron densities. In Fig. 6 the FWHM, obtained by our simulation technique for the electron density interval $10^{15} - 10^{16} \text{ cm}^{-3}$ and for two temperatures (10 000 and 15 000 K), are compared with the corresponding data of Stehle and Hutcheon [11] and our quasistatic results. Also included are the data of Döhrn *et al.* [4], Castell *et al.* [2], and our experimental results. As can be seen, our FCSM α values are systematically larger compared to the data of Ref. [11] (about 3%) and the results of the quasistatic approach (about 10%). At higher electron densities, the agreement between our calculations and measurements can be regarded as satisfactory. Such small discrepancies between FWHMs are not surprising because (as discussed in Sec. IV) for most parts of the P_β line profile, the quasistatical approximation for ions and the impact approximation for electrons are well fulfilled. The FCSM calculation yields the largest widths while the quasistatic approach the lowest. It is also worth stressing that the P_β line shape is formed mainly by interactions with ions, which contribute to the FWHM about three times more than the interactions with electrons. In the electron density range of our experiments, this proportion is fulfilled with an accuracy better than 5%

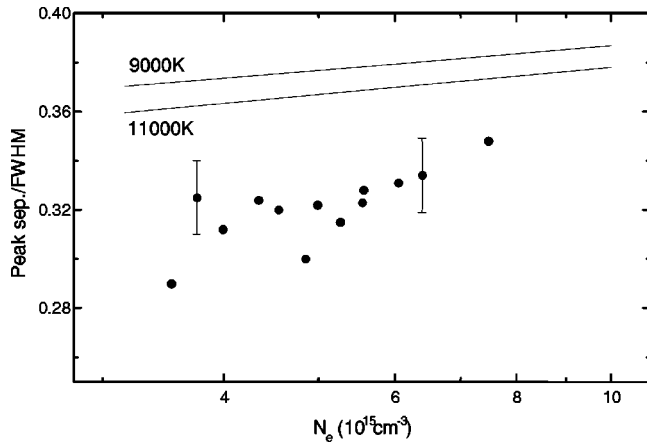


FIG. 7. Measured and calculated ratios of the peak separation to the FWHM versus the electron density of the plasma. The solid circles represent the measured values; the lines our FCSM calculations for two temperatures.

for all theoretical approaches discussed in Fig. 6.

In Fig. 7 we compare our measured and calculated ratios of the peak separation to the FWHM. As can be seen, our theoretical data systematically exceed the measured values.

In Fig. 8 the measured dip values defined as $Dip = 1 - 2J_{Dip}/(J_v + J_r)$ are compared with calculated ones for two temperatures 9000 K and 11 000 K. The symbols J_v and J_r correspond to intensities of the violet and the red shoulder, while the J_{Dip} to the dip intensity. For electron densities of our experiments, the theoretical data exceed systematically the observed dip values by about a factor of 1.5.

We want to emphasize that the character of the experiment-theory discrepancy, shown in Figs. 5–8 is similar—the measurements systematically yield smaller values than calculations. Such discrepancy may be interpreted as follows: to our measured spectral line intensity distribution, beside the radiation originating from homogeneous plasma layers (with given N_e and T), the radiation from

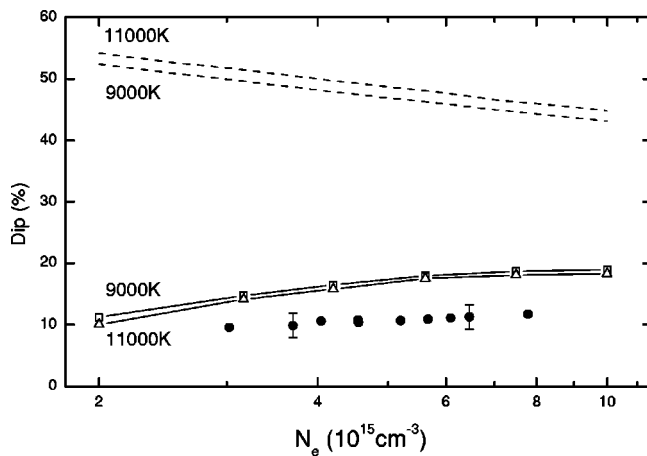


FIG. 8. Comparison of our measured (solid circles) and calculated dip values as a function of the electron density. Results obtained within two approaches are shown: the FCSM (solid lines) and the quasistatic approximation (dashed lines), both for two temperatures.

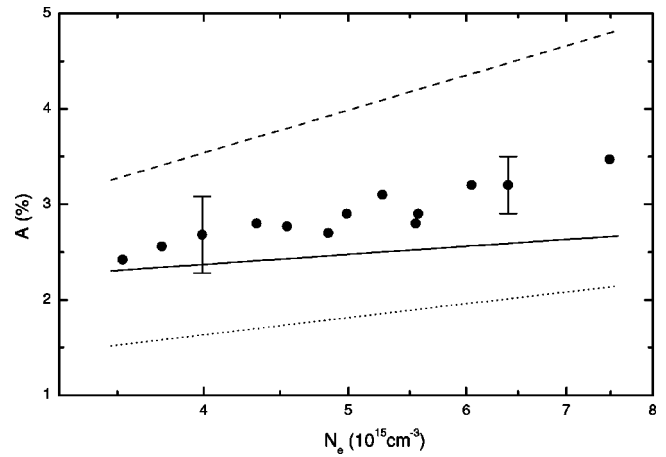


FIG. 9. The asymmetry parameter of the shoulder intensity A plotted against the electron density of the plasma. The solid circles represent the experimental data, the solid line our calculations, the dashed line the theoretical results of Ref. [31], and the dotted line our quasistatic approximation.

plasma layers with lower electron densities and temperatures slightly contributes. This is reflected in filling up the line dip and in shifting the line shoulders slightly towards the line center as well as increasing their intensities. Consequently, the observed FWHM are systematically somewhat smaller. We estimate that the possible resulting error reaches 5–10 % of the FWHM for the high and low N_e conditions, respectively. Fortunately, these effects do not influence significantly the asymmetry parameter and the line shift, because in these “disturbing” cooler plasma layers the electron densities are substantially lower.

In Fig. 9 the quantity $A = 2 \times (J_v - J_r)/(J_v + J_r)$, routinely used as a measure of asymmetry of β -like transitions in hydrogen, is plotted against the electron density. As can be seen, the measured A values are systematically larger than

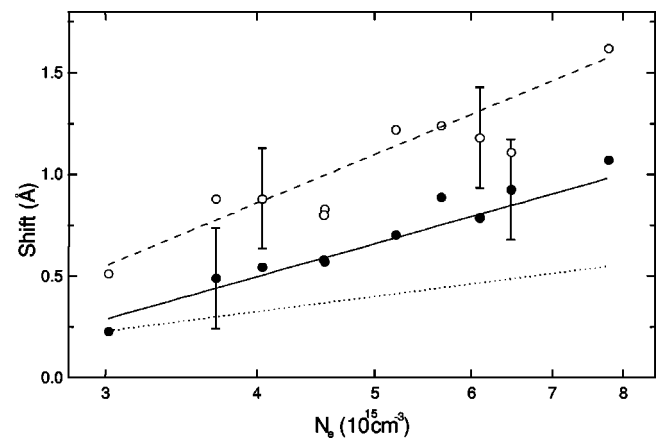


FIG. 10. Comparison of measured (symbols) and calculated (lines) P_β shifts determined (a) at the half maximum intensity level ($\delta\lambda_{1/2}$) and (b) for the dip position ($\delta\lambda_{Dip}$). The solid and open circles are for the $\delta\lambda_{1/2}$ and $\delta\lambda_{Dip}$, respectively. The solid line represents the results of our $\delta\lambda_{1/2}$ calculations. Theoretical data of Ref. [31] for the $\delta\lambda_{1/2}$ (dashed line) and $\delta\lambda_{Dip}$ (dotted line) are shown for comparison.

those resulting from our calculations, however, the discrepancies do not exceed 15%. In addition, we compare in Fig. 9 our results with asymmetry parameters resulting from our quasistatic approximation and from the approach of Ref. [31]. As can be seen, the quasistatic data are significantly smaller than our simulated results, despite the fact that—according to the inequality [Eq. (9)]—the criterion of quasistatic approximation for our plasma conditions is fulfilled for wavelength separations corresponding to the positions of the P_β line peaks. This discrepancy between our simulated results and the quasistatic data results from ion dynamic effects, which cause the increase in the dip intensity and simultaneously the decrease in the shoulder intensity. On the other hand, the asymmetry parameters resulting from the approach of Ref. [31] systematically exceed our measured data nearly by a constant factor of 1.4.

In Fig. 10 the measured and calculated P_β line shifts are shown as a function of electron density of the plasma. Two quantities characterizing the line shift are presented: (i) the so-called dip shift $\delta\lambda_{Dip}$ and (ii) the shift determined at the half intensity maximum of the profile $\delta\lambda_{1/2}$. Both above-mentioned shifts have been determined by Günter and Könies [31]. Within their quantum statistical approach, the dip shift is almost entirely caused by electron collisions, because the central part of the profile is formed by weak ionic electric fields. The shift $\delta\lambda_e$ caused by electron collisions amounts to about 90% of the total dip shift $\delta\lambda_{Dip}$. We have obtained our $\delta\lambda_{1/2}$ shifts from Eq. (5), taking the electronic contribution $\delta\lambda_e$ from Ref. [31].

In conclusion, we want to point out that in the case of the P_β line:

(i) All theoretical approaches yield nearly the same FWHM of the P_β line. Our simulation technique yields the

largest FWHM, exceeding the quasistatic data by about 10%.

(ii) The quasistatic approach as well as the MMM [11] do not describe satisfactorily the central part of the line profile.

(iii) Our theoretical results for the FWHM, the ratio (Peak sep/FWHM) and the dip value are systematically slightly larger than the respective measured parameters. In our opinion, this discrepancy is mainly caused, as mentioned earlier, by the departure of our plasma from homogeneity.

(iv) The calculated P_β line shape parameters, the asymmetry (A) and the line shift ($\delta\lambda_{1/2}$), agree well with the corresponding measured data.

(v) Finally, we want to stress the satisfactory agreement between our measured dip shifts and the shifts obtained by Günter and Könies in the frame of the quantum statistical approach using the Green's function technique. This approach seems to provide reliable shifts caused by electronic collisions, whereas the semiclassical approaches [30] yield questionable results. On the other hand, the theory [31] yields $\delta\lambda_{1/2}$ shifts that are too small compared to the measured data. This discrepancy indicates that the ionic (*violet*) shift calculated by Günter and Könies is overestimated. The overestimation of the ionic interaction is consistent with the observed discrepancy between the asymmetry parameters A —the measured peak asymmetries are significantly smaller than those resulting from the approach of Ref. [31].

ACKNOWLEDGMENTS

We would like to thank S. Günter and A. Könies for supplying us with the P_β line profiles corresponding to our plasma conditions.

-
- [1] G. Hepner, *Spectrochim. Acta* **11**, 356 (1957).
 [2] R. Castell, D. Mandelbaum, A. Mendez, and A. Sanchez, *J. Quant. Spectrosc. Radiat. Transf.* **30**, 345 (1983).
 [3] A. Döhrn, Ph.D. thesis, Christian-Albrechts-Universität, Kiel, 1995.
 [4] A. Döhrn, P. Nowack, A. Könies, S. Günter, and V. Helbig, *Phys. Rev. E* **53**, 6389 (1996).
 [5] O. Motapon, M.G. Kwato Njock, B. Oumarou, and N. Tran Minh, *J. Phys. B* **30**, 3117 (1997).
 [6] O. Vallée, J. Picart, and N. Tran Minh, *J. Phys. B* **17**, L565 (1984).
 [7] J. Szudy and W.E. Baylis, *J. Quant. Spectrosc. Radiat. Transf.* **15**, 641 (1975).
 [8] P. Kepple and H.R. Griem, *Phys. Rev.* **173**, 317 (1968).
 [9] C.R. Vidal, J. Cooper, and E.W. Smith, *Astron. Astrophys., Suppl. Ser.* **25**, 37 (1973).
 [10] C. Stehle, *Phys. Scr., T* **65**, 183 (1996).
 [11] C. Stehle and R. Hutcheon, *Astron. Astrophys., Suppl. Ser.* **140**, 93 (1999).
 [12] (a) V. Cardenoso and M.A. Gigosos, *J. Phys. B* **20**, 6005 (1987); (b) *Phys. Rev. A* **39**, 5258 (1989); (c) M.A. Gigosos and V. Cardenoso, *J. Phys. B* **29**, 4795 (1996).
 [13] J. Halenka and W. Olchawa, *J. Quant. Spectrosc. Radiat. Transf.* **56**, 17 (1996).
 [14] G.C. Hegerfeldt and V. Kesting, *Phys. Rev. A* **37**, 1488 (1988).
 [15] V. Kesting, Ph.D. thesis, Georg-August-Universität, Göttingen, 1992.
 [16] S. Alexiou, A. Calisti, P. Gauthier, L. Klein, E. Leboucher-Daimler, R.W. Lee, R. Stamm, and B. Talin, *J. Quant. Spectrosc. Radiat. Transf.* **58**, 399 (1997).
 [17] S. Alexiou, P. Sauvan, A. Poquerrusse, E. Leboucher-Dalimier, and R.W. Lee, *Phys. Rev. E* **59**, 3499 (1999).
 [18] S. Günter, L. Hitzschke, and G. Röpke, *Phys. Rev. A* **44**, 6834 (1991).
 [19] S. Günter, *Phys. Rev. E* **48**, 500 (1993).
 [20] S. Günter and A. Könies, *Phys. Rev. E* **55**, 907 (1997).
 [21] W. Olchawa, Ph.D. thesis, Nicholas Copernicus University, Toruń, 1997.
 [22] R. Stamm and D. Voslamber, *J. Quant. Spectrosc. Radiat. Transf.* **22**, 599 (1979).
 [23] R. Stamm, E.W. Smith, and B. Talin, *Phys. Rev. A* **30**, 2039 (1984).
 [24] J. Seidel and R. Stamm, *J. Quant. Spectrosc. Radiat. Transf.* **27**, 499 (1982).

- [25] S. Sorge and S. Günter, *Eur. Phys. J. D* **12**, 369 (2000).
- [26] J. Halenka, *Z. Phys. D: At., Mol. Clusters* **16**, 1 (1990).
- [27] E.W. Smith, *Phys. Rev.* **166**, 102 (1968).
- [28] W.H. Press, S.A. Teukolsky, W.T. Vetterling, and B.P. Flannery, *Numerical Recipes in FORTRAN*, 2nd ed. (Cambridge University Press, New York, 1992).
- [29] C.A. Iglesias, D.B. Boercker, and R.W. Lee, *Phys. Rev. A* **32**, 1906 (1985).
- [30] H.R. Griem, *Phys. Rev. A* **28**, 1596 (1983); **38**, 2943 (1988).
- [31] S. Günter and A. Könies (private communication).
- [32] S. Alexiou, in *Spectral Line Shapes*, edited by J. Seidel (API, Berlin, 2000), Vol. 11, p. 135.
- [33] C.F. Hooper, Jr., *Phys. Rev.* **165**, 215 (1968).
- [34] H.R. Griem, *Spectral Line Broadening by Plasmas* (Academic Press, New York, 1974).
- [35] T. Wujec, A. Baclawski, A. Golly, and I. Książek, *Acta Phys. Pol. A* **96**, 333 (1999).
- [36] J. Musielok, W.L. Wiese, and G. Veres, *Phys. Rev. A* **51**, 3588 (1995).
- [37] J. Musielok, *J. Tech. Phys.* **15**, 259 (1999).
- [38] H.R. Griem, *Plasma Spectroscopy* (McGraw-Hill, New York, 1964).
- [39] W.L. Wiese, J.R. Fuhr, and T.M. Deters, *J. Phys. Chem. Ref. Data Monogr.* **7**, 157 (1996).